Available online at www.sciencedirect.com

ScienceDirect

Advances in Space Research 73 (2024) 4175–4186

ADVANCES IN SPACE RESEARCH (a COSPAR publication)

www.elsevier.com/locate/asr

Multi-GNSS Precise Point Positioning enhanced by the real navigation signals from CENTISPACE™ LEO mission

Shengyi Xu [a], Qiangwen Yang [b], Xiaodong Du [b], Xiaolong Xu [a,*], Qile Zhao [a], Long Yang [b], Yanan Qin [b], Jing Guo [a,*]

[a] GNSS Research Center, Wuhan University, No. 129 Luoyu Road, 430079 Wuhan, China
[b] Beijing Future Navigation Tech Co. Ltd, Beijing 100081, China

Received 12 September 2023; received in revised form 6 January 2024; accepted 9 January 2024
Available online 11 January 2024

Abstract

The Low Earth Orbit (LEO) satellites can significantly reduce the convergence time of Precise Point Positioning (PPP), as the rapid motion of LEO satellites leads to the fast changes of the observation geometry. This helps to accelerate the separation of ambiguity as well as receiver's positions. In this study, the real dual-frequency navigation signals of the CENTISPACE™ ESAT1 satellite are used to enhance the Multi-GNSS Precise Point Positioning (PPP). The onboard GPS, Galileo and BDS-3 observations are used to derive the precise orbits of ESAT1, while the clock is determined based on the data from a ground network established by Wuhan University. With them, the impact of the ESAT1 on float PPP with single, dual, and three constellations (GPS-only, Galileo-only, BDS-3 only, GPS/-Galileo, GPS/BDS-3, Galileo/BDS-3, and GPS/Galileo/BDS-3) is analyzed in terms of convergence time and positioning accuracy. The analysis reveals that the average convergence time in the east direction is reduced by 7.9, 2.4, 12.0, 2.0, 3.4, 2.6 and 1.3 min respectively. Additionally, the 3D accuracy improves around 3.2, 4.1, 5.8, 1.1, 0.3, 1.5 and 0.6 cm respectively. Furthermore, the contribution of ESAT1 observations for Mult-GNSS PPP with Ambiguity Resolution (PPP-AR) is also investigated. The average Time to First Fix (TTFF) of each solution can be reduced about 8.1, 5.2, 4.9, 1.3, 0.9, 1.1 and 0.4 min, respectively. Overall, the PPP and PPP-AR are benefited with LEO signals, in particularly for the single-system solutions, and the results demonstrate the promising contribution of LEO on high-accuracy positioning.

Keywords: CENTISPACE™ LEO Constellation; LEO-augmented GNSS; Precise Point Positioning (PPP); Convergence time; Positioning accuracy

1. Introduction

Nowadays, there are more than 120 navigation satellites to provide global positioning, navigation, and timing (PNT) services. However, as their orbit altitude exceeds 20,000 km, the signal strength is prone to be weak during the transmission, especially in obscured environments. In contrast, Low Earth Orbit (LEO) satellites operating at orbit altitudes typically between 400 and 1500 km, can provide stronger signals compared to distant GNSS satellites (Enge et al., 2012). This translates to stronger signals and better anti-jamming as well as anti-spoofing capabilities. Moreover, LEO satellites have the advantage of rapid motion, allowing for rapid changes in the geometric configuration. This can speed up the separation of parameters, especially in terms of position and ambiguity (Li et al., 2022a; Zheng et al., 2023). It enables Precise Point Positioning (PPP) to achieve centimeter-level within one or two minutes by its combination with the current Global Navigation Satellite System (GNSS), i.e., the United

* Corresponding authors.
E-mail addresses: xlxu@whu.edu.cn (X. Xu), jingguo@whu.edu.cn (J. Guo).

https://doi.org/10.1016/j.asr.2024.01.017
0273-1177/

States' Global Position System (GPS), Russia's GLObal NAvigation Satellite System (GLONASS), the European Union's Galileo and China's BeiDou Navigation Satellite System (BDS) (Li et al., 2019a; Zhao et al., 2020). Moreover, with 240 LEO satellites, convergence within 1 min can be achieved (Ge et al., 2022). Hence, independent or enhanced navigation with LEO constellation is redrawn more attention in the field of navigation technology, after about five decades, when the success of United States' Transit system.

However, LEO satellites cover only one tenth of the Earth's surface compared to the current GNSS navigation satellites (Enge et al., 2012). Hence, nearly one hundred LEO satellites are needed to be deployed to achieve similar Earth surface coverage as ten MEO satellites (Chobotov, 2002; Ge et al., 2022). Fortunately, with technical advancements in satellite construction as well as the launch, the costs for LEO constellation are reduced dramatically. Hence, the huge LEO constellations can be established with economic cost. The Iridium constellation, including its subsequent Iridium NEXT, is one of the most notable examples (Fossa et al., 1998). The constellation provides not only the satellite communication service, but also the Satellite and Timing Service (STL) to service as alternative PNT of GPS. As an independent PNT source, the higher radio power and signal coding gain are used, the STL signals are able to penetrate into difficult attenuation environments to provide 10 m-level positioning. In addition, several internationally recognized companies such as Boeing (Selding, 2016), SpaceX (McDowell, 2020), Oneweb (Jewett, 2020) from the United States, Telesat (Hill, 2020), Kepler Communications (Harebottle, 2018) from Canada, Astrome (Nyirad, 2019a) from India, Astrocast (Nyirady, 2019b) from Switzerland, Samsung (Magan, 2015) from Korea, Hongyan (Meng et al., 2018), Hongyun (CNAGA, 2017), and CENTISPACE^{TM} (Jones, 2018) from China, have proposed plans to establish their own LEO constellations. These constellations aim to not only provide global broadband Internet services, but also have the potential to offer independent or enhanced PNT service. Reid et al., (2016a,2016b) have extensively explored the possibilities and implementation strategies for independent LEO navigation satellite system.

Different with Iridium, the LEO constellation can also broadcast the compatible signals with current GNSS constellations to enhance their PNT ability. This can reduce the count of necessary LEO satellites, while fast and high accuracy positioning can be ensured on a global scale, and already draw more attention within GNSS community. Many scholars have conducted simulation study to evaluate LEO's impact on enhancing GNSS positioning performance across various scenarios. Ke et al., (2015) tested the enhancement performance of 48 LEO satellites for GNSS PPP. Compared to GPS-only, the GPS/LEO combined PPP with Ambiguity Resolution (PPP-AR) demonstrates a 51.31 % reduction in convergence time and a 14.9 % improvement in positioning accuracy. Additionally, the convergence time of GPS/GLONASS combined PPP-AR is reduced by 3.93 %, indicating that LEO satellites play a more significant role in accelerating the convergence of PPP compared to Medium Earth Orbit (MEO) satellites. Ge et al. (2018) utilized 66 simulated LEO satellites and found that LEO enhanced GNSS could reduce the convergence time of PPP to just 5 min. The results by Li et al., (2019b) showed that the convergence time of multi-GNSS PPP could be reduced from 9.6 to 7.0, 3.2, 2.1, and 1.3 min with the 60, 96, 192, and 288 LEO satellites, respectively. Li et al. (2021) utilized a constellation of 150 LEO satellites and demonstrated that the combination of the BDS and LEO significantly reduced the convergence time of PPP by approximately 20 times. Moreover, they achieved decimeter-level precision in just 1 min. Hong et al. (2023) simulated 180 LEO satellites to evaluate their contribution to the convergence of PPP and PPP-AR. The convergence of PPP solution is improved by more than 90 % and the Time-To-First-Fix (TTFF) can be reduced by more than 80 %. Besides PPP, Ge et al. (2022) also confirmed the feasibility of LEO constellation for precise orbit determination (POD) of GNSS satellites, highlighting its advantages and challenges in POD, precise clock determination, estimation of earth rotation parameters (ERP), and global ionospheric modelling (GIM). It is worth noting that all of the aforementioned studies are based on simulated data.

Luojia-1A satellite operated by Wuhan University is the LEO satellite with GNSS enhanced ability. The Luojia-1A navigation augmentation system is capable of providing useable LEO navigation augmentation signals to integrate with existing GNSS to improve the real-time navigation performance. Wang et al. (2019) verified that the precision reaches 0.7 m and 0.8 m respectively for the dual frequency pseudorange measurements and the carrier phase precision is 2.8 mm and 2.6 mm respectively by the zero-baseline approach. However, there is no available information to confirm the contribution of LuoJia-1A to PPP. Although the first experimental satellite has been launched for the "Hong Yan" constellation by China Aerospace Science and Technology Corporation (CAST) as well as the "Hong Yun" project by China Aerospace Science and Industry Corporation. No public information on the performance can be found. Besides, Beijing Future Navigation Tech Co., Ltd has already launched its CENTISPACE^{TM} LEO navigation constellation since in 2018. Currently, there are five experimental satellites successfully deployed. A ground network with dedicated receiver developed and provided by Beijing Future Navigation Tech Co., Ltd has been established by GNSS Research Center of Wuhan University to track their signals and assess the performance.

In this study, the real tracking data from ground stations are used to assess the contribution of CENTISPACE^{TM} LEO experimental satellite to Multi-GNSS PPP. Following the introduction of GNSS and LEO combined PPP algorithm, the information about the

CENTISPACE™ constellation as well as the ground tracking data are presented. Afterwards, the performance of LEO enhanced Multi-GNSS PPP is investigated and analyzed with the metrics of convergence time and accuracy. LEO satellites' contribution to GNSS PPP-AR is further explored. Finally, the study is concluded.

2. PPP with multi-GNSS and LEO constellation

The GNSS observation models for the ionosphere-free (IF) combination of dual-frequency pseudorange and carrier phase in the unit of length can be written as follows,

$$\begin{aligned}\rho_r^{S,k} &= R_r^{S,k} + c\delta t_r - c\delta t^{S,k} + m_r^{S,k}T_r + d_r^{S,k} - d^{S,k} + \varepsilon_{\varrho,r}^{S,k}\\ \phi_r^{S,k} &= R_r^{S,k} + c\delta t_r - c\delta t^{S,k} + m_r^{S,k}T_r + \lambda_{IF}N_{r,IF}^{S,k} + b_r^{S,k} - b^{S,k} + \varepsilon_{\phi,r}^{S,k}\end{aligned} \tag{1}$$

where $\rho_r^{S,k}$ and $\phi_r^{S,k}$ denote the IF pseudorange and carrier phase measurement between satellite k of the GNSS system S and station r, S can be either "G" for GPS, "E" for Galileo, or "C" for BDS-3; $R_r^{S,k}$ is the geometry distance between the satellite and station; c is the speed of light in vacuum; δt_r and $\delta t^{S,k}$ are the clock errors for station r and satellite k; $m_r^{S,k}$ denotes the mapping function of the troposphere delay, while T_r is the zenith troposphere delay on station r; $d_r^{S,k}$ and $d^{S,k}$ denote the frequency-dependent pseudorange hardware biases at station r and satellite k, respectively, while $b_r^{S,k}$ and $b^{S,k}$ are their counterparts for phase, all of which are presumed time-constant; and λ_{IF} indicates the wave length of narrow-lane ambiguity; $N_{r,IF}^{S,k}$ represents the IF ambiguity; $\varepsilon_{\varrho,r}^{S,k}$ and $\varepsilon_{\phi,r}^{S,k}$ are the IF pseudorange and phase observation noise, respectively. For brevity, phase centre variation, phase windup, relativistic effects, and tide corrections are omitted.

Given that the LEO constellation broadcasts the L-band signals for navigation and enhancement of the current GNSS, Equ. (1) can also be used to model the pseudorange and carrier phase measurements from LEO satellite, by simply taking the superscript 'S' as 'L'. For multi-GNSS data analysis, there is one inter-system bias to be estimated to account for the different pesudorange bias in the receiver side. Hence, for the combination of LEO and GNSS, the inter-system bias (ISB) should also be modelled. By taking the GPS as the reference, the Equ (1) can be rewritten as follows for GPS and other GNSS as well as LEO constellation,

$$\begin{aligned}\rho_r^{G,k} &= R_r^{G,k} + c\delta\tilde{t}_r - c\delta\tilde{t}^{G,k} + m_r^{G,k}T_r + \varepsilon_{\varrho,r}^{G,k}\\ \phi_r^{G,k} &= R_r^{G,k} + c\delta\tilde{t}_r - c\delta\tilde{t}^{G,k} + m_r^{G,k}T_r + \lambda_{IF}N_{r,IF}^{G,k}\\ &\quad + \left(b_r^{G,k} - b^{G,k} - d_r^{G,k} + d^{G,k}\right) + \varepsilon_{\phi,r}^{G,k}\end{aligned} \tag{2}$$

$$\begin{aligned}\rho_r^{S,k} &= R_r^{S,k} + c\delta\tilde{t}_r - c\delta\tilde{t}^{S,k} + m_r^{S,k}T_r + ISB^{S,G} + \varepsilon_{\varrho,r}^{S,k}\\ \phi_r^{S,k} &= R_r^{S,k} + c\delta\tilde{t}_r - c\delta\tilde{t}^{S,k} + m_r^{S,k}T_r + \lambda_{IF}N_{r,IF}^{S,k}\\ &\quad + \left(b_r^{S,k} - b^{S,k} - d_r^{S,k} + d_r^{G}\right) + ISB^{S,G} + \varepsilon_{\phi,r}^{S,k}\end{aligned} \tag{3}$$

where $\delta\tilde{t}_r = c\delta t_r + d_r^{S,k}$ and $\delta\tilde{t}^{S,k} = c\delta t^{S,k} + d^{S,k}$; $ISB^{S,G}$ denotes the ISB between the GPS and other GNSS or LEO system.

As the IF combination used for the data procession, the wide-lane (WL) and narrow-lane (NL) ambiguities are fixed sequentially. For the WL ambiguity resolution, the Melbourne-Wubbena (MW) combination is used,

$$N_{r,WL}^{S,k} = \left(\frac{L_{r,1}^{S,k}}{\lambda_1} - \frac{L_{r,2}^{S,k}}{\lambda_2}\right) - \frac{f_1P_{r,1}^{S,k} + f_2P_{r,2}^{S,k}}{(f_1+f_2)\cdot\lambda_w} \tag{4}$$

where $N_{r,WL}^{S,k}$ denotes the WL ambiguity and λ_w denotes the WL wavelength; f denotes the signal frequency; $P_{r,i}^{S,k}$ and $L_{r,i}^{S,k}$ denote the raw pseudorange and carrier phase measurement at the i frequency. The bootstrapping strategy proposed by Dong and Bock (1989) has been employed to fix each WL ambiguities. With the fixed WL ambiguity $\bar{N}_{r,WL}^{S,k}$ as well as the estimate of the float IF ambiguity $N_{r,IF}^{S,k}$, the NL float ambiguities $N_{r,NL}^{S,k}$ are derived.

$$N_{r,NL}^{S,k} = \frac{f_1+f_2}{f_1}N_{r,IF}^{S,k} - \frac{f_2}{f_1-f_2}\bar{N}_{r,WL}^{S,k} \tag{5}$$

Afterwards, the LAMBDA algorithm (Teunissen, 1995) is used for fixing the NL ambiguities, and the ratio test is applied for validation.

In general, integer ambiguity resolution can improve the accuracy of the positioning, particularly in the east direction. However, the positioning performance may degenerate under the conditions of poor ambiguity precision which gives a low fixed rates of full ambiguity resolution (Parkins, 2011). Hence, partial ambiguity resolution (PAR) has been proposed to provide accurate and continuous positioning solutions, and the strategy is introduced in the next section.

3. Data processing

3.1. CENTISPACE™ LEO constellation

The CENTISPACE™ mission is designed and developed by Beijing Future Navigation Tech Co., Ltd, which aims at providing global LEO-based augmentation positioning and navigation services. According to the construction plan, the formal constellation will be formed by about 160 LEO satellites. Before that, several experimental satellites have been already launched during last few years for onboard validation of key techniques. The first experimental satellite was launched in 2018, while another four were launched from September to October 2022.

The last four experimental satellites are placed at a same orbit altitude, corresponding to a typical pass of 5–15 min for ground receivers. By deliberate configuration of their orbit inclinations and in-plane phase offsets, a maximum observation window of approximately 5 min is made possible to simultaneously track the four experimental satellites,

thus providing opportunities to assess the LEO augmentation performance with multiple LEO satellites.

3.2. Ground tracking data

In order to assess the observation quality as well as the enhanced performance of CENTISPACE^{TM} experimental satellites, a regional network consisted of seven stations located around Hubei Province, China, have been established by GNSS Research Center of Wuhan University. Beijing Future Navigation Tech Co., Ltd. provides core receivers for the seven stations and authorizes Wuhan University to analyze and process the data generated by the receivers. Fig. 1 shows their distribution.

The precise orbits of ESAT1 were determined with the data provided by Beijing Future Navigation Tech Co., Ltd., and only the data on January 1, 2023 are used in this study, considering the integrity of the data.

Fig. 2 illustrates the trajectory of the ESAT1 satellite's subsatellite points as well as the location of the regional ground network on January 1, 2023. It clearly reveals that the satellite's motion is confined within −60 and 60 region of latitudes, and only small part of the trajectory can be tracked by the stations. For the tracking length of the seven ground stations on ESAT1, the longest is around 15 min in theory, and the gap between arcs is about 100 min, as the orbital period is around 96 min. In addition, the low altitude of LEO makes the elevation angle between the arcs vary significantly, thus noticeable difference on tracking can be expected. Among the seven stations, stations 6101, 6103, and DG07 demonstrated better tracking capability of the ESAT1 satellite, while station 6229 shows the worst performance due to greater occlusion around the station. Table 1 presents the average PDOP values and the average number of satellites for each constellation at each station. On average, the number of satellites tracked for the GPS, Galileo, and BDS-3 constellations are 8.18, 6.62, and 7.96, respectively. The GPS system exhibits the best geometrical configuration, while the Galileo system shows the least favorable configuration.

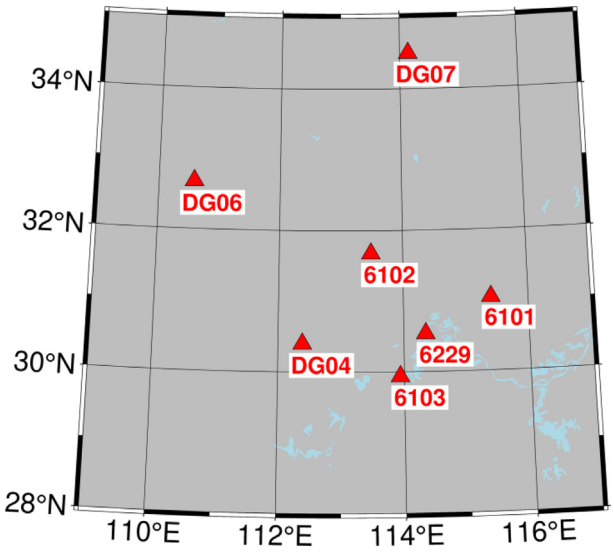

Fig. 1. Distribution of the ground tracking stations.

Fig. 3 further shows the sky plots of GPS, Galileo, BDS-3 and ESAT1 satellite during (a) 10 min as well as (b) 24 h for DG07. In Fig. 3(a), the geometric changes of ESAT1 are over ten times quicker than that of GNSS satellites, which indicates that the addition of ESAT1 satellite can accelerate the change of geometric configuration. It is crucial for the fast convergence of PPP. The maximum elevation increases from around 15 to 45 degrees. However, stronger multipath should be expected for ESAT1 in the lower elevation. We also can observe that the passing time of ESAT1 is shorter than that of GNSS satellites due to the fast motion of LEO satellite. In addition, GNSS satellites are mainly distributed in the south hemisphere of the sky plot. The inclusion of ESAT1 increases the observability in the north hemisphere, and effectively improves the geometric configuration of the navigation system.

3.3. Data processing strategy

The PPP is employed for analysing the ESAT1′s contribution to the performance of Multi-GNSS PPP. PPP is relied on the precise orbit and clock products. For Multi-GNSS, the final WUM products from the Wuhan University Analysis Center of International GNSS Service Multi-GNSS Experiment are used (Guo et al., 2023), and they are also used to determine the ESAT1 precise orbits provided by Beijing Future Navigation Tech Co., Ltd. We redetermine the clock based on the ground tracking data by fixing the orbit determined with onboard GNSS observables. Finally, the derived LEO orbit and clock are combined with WUM final products for PPP.

Table 2 summarizes the employed strategy in details. In the analysis, we perform the PPP for each constellation as well as the combination of two or three with or without CENTISPACE^{TM} ESAT1 satellite. The single constellation schemes include GPS (G), Galileo (E), and BDS-3 (C), while the dual-system combined schemes are GPS/Galileo (GE), GPS/BDS-3 (GC), and Galileo/BDS-3 (EC). The L1/L2, E1/E5a, B1I/B3I, and L1/L5 are employed for GPS, Galileo, BDS-3, and ESAT1. As no phase center corrections for receivers available in the legacy IGS antenna file, those are assumed as zero for all systems. On the transmitter side, the phase center corrections in IGS antenna file are applied for Multi-GNSS satellites, while the phase center offsets from manufacture are corrected for ESAT1 with zero phase center variations. The TurboEdit algorithm (Blewitt, 1990) is used for data quality control. However, as the rapid motion of the ESAT1 satellite causes significant changes of ionospheric delay, the threshold value of geometry-free (GF) combination for cycle slip detection is set relative larger, e.g., 5 cycles. The carrier phase noise of each frequency for all constellations is set to 2 cm with an empirical code-to-carrier ratio of 100:1. To weak the multipath effect of low-elevation observations,

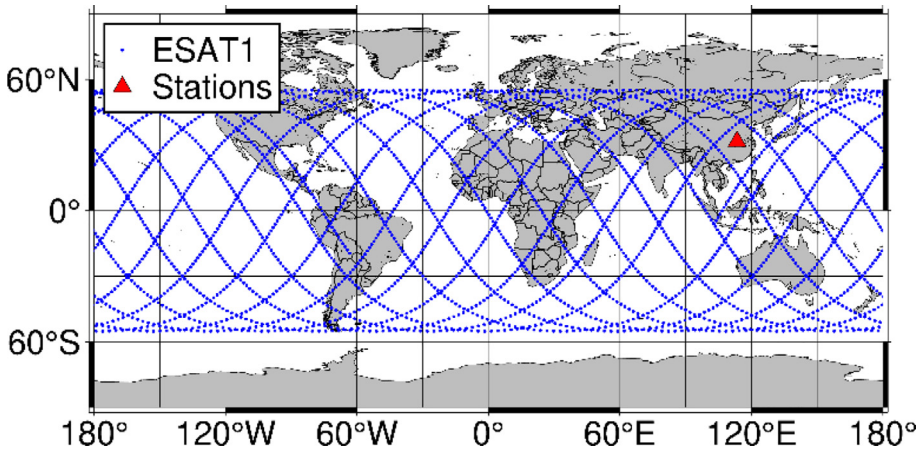

Fig. 2. The trajectory of the ESAT1 satellite's subsatellite points as well as the location of the regional ground network on January 1, 2023.

Table 1
The average effective number of constellation and PDOP value for each tracking station.

Station	Satellite number			PDOP		
	GPS	Galileo	BDS-3	GPS	Galileo	BDS-3
6101	8.61	7.14	8.23	1.10	1.25	1.15
6102	8.53	6.84	8.21	1.11	1.30	1.15
6103	8.43	6.98	8.26	1.11	1.27	1.14
6229	6.45	4.78	6.64	1.47	2.38	1.79
DG04	8.50	6.60	8.21	1.11	1.30	1.15
DG06	8.29	6.85	8.02	1.13	1.41	1.18
DG07	8.46	7.13	8.12	1.12	1.27	1.17
Mean	8.18	6.62	7.96	1.16	1.45	1.25

we adopt an elevation-dependent function for weighting, i.e., $(2 \cdot \sin(ele))^2$ for satellites with elevation lower than 30° and 1.0 for those above 30 degrees. Moreover, the mask elevation is set as 10 degrees. For the combined solutions, the ISB parameters are estimated as constants for each non-reference system as well as ESAT1. This avoids the rank deficiency of estimation for LEO constellation.

In terms of ambiguity, the PPP solutions with or without integer ambiguity resolution are all investigated although only one LEO satellite is used where only the ambiguities of multi-GNSS are tried to fix. To eliminate receiver-related biases, single-difference WL and NL ambiguities are formed before performing PPP-AR. We resolve the WL ambiguity for each satellite using the integer bootstrapping method (Dong and Bock, 1989). The derivation, sigma, and decision function of the WL ambiguity are configured as 0.15 cycle, 0.1, and 1000, respectively. The successfully resolved WL ambiguities are then used to calculate the NL ambiguities. Next, we resolve the NL ambiguities using the LAMBDA algorithm (Teunissen, 1995). Ambiguity verification is conducted using a ratio test with a threshold of 2.0. As it is not possible to successfully fix all NL ambiguities, PAR is applied. Although there are the various ways of implementing PAR, such as based on elevation angle (Li et al., 2014), decorrelation variance (Li et al., 2022b), etc., we utilize a traversal method to select the fixed NL ambiguities subset. In the first step, the number of NL ambiguities to be deleted are

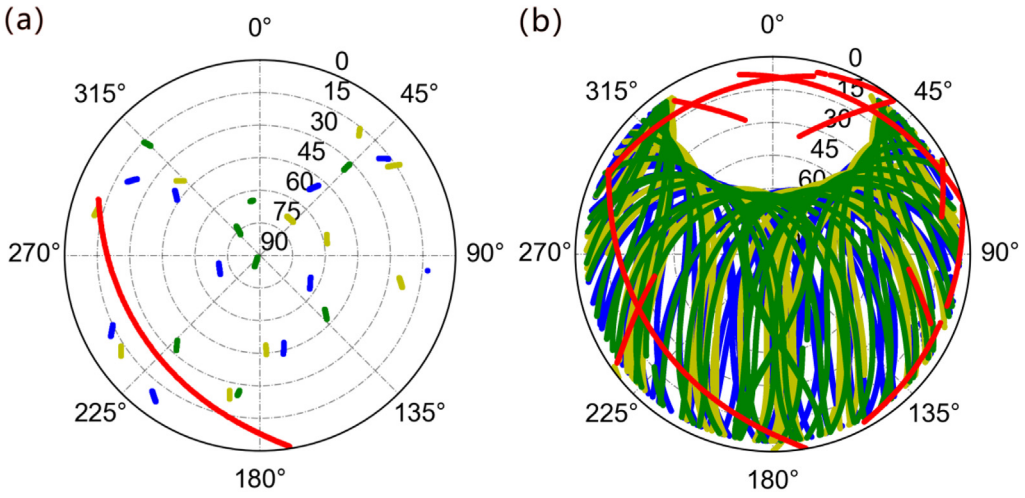

Fig. 3. The sky plots of GPS (blue), Galileo (green), BDS-3 (yellow) and ESAT1 (red) satellites during (a) 10 min as well as (b) 24 h for DG07.

Table 2
Strategy for PPP based on the measurements from Multi-GNSS and ESAT1.

Items	Description
Constellation	GPS, Galileo, BDS-3, and CENTISPACE^{TM} ESAT1
Signal	GPS:L1/L2; GAL:E1/E5a; BDS-3:B1I/B3I; LEO:L1/L5
Observations	IF for PPP
Estimator	Square Root Information Filter (SRIF)
Intervals	2 s
Elevation mask	10°
Cycle slip detection	TurboEdit algorithm (Blewitt, 1990)
Solid tide, ocean tide	Corrected according to IERS Convention 2010
Satellite PCO/PCV	GNSS: Corrected according to IGS20_2239.ATX ESAT1: Manufacture values for PCO and zero PCVs
Receiver PCO/PCV	None
Stochastic model	An elevation-dependent function, where b is the nominal noise. $\sigma^2_{ele} = \begin{cases} b^2 & ele > 30^\circ \\ \frac{b^2}{4\sin^2\theta} & ele \le 30^\circ \end{cases}$
Relativistic effect	Corrected
Phase-windup	Corrected
ISB	Estimated as a constant
Satellite orbit	WUM final products for GNSS Onboard GNSS determined orbits for ESAT1
Satellite clock	WUM final products for GNSS Ground tracking data determined clock for ESAT1
Troposphere delay	Saastamoninen model (Saastamoinen, 1972) and PWC estimation, with priori sigma of 0.2 m and random-walk process noise $0.02m/\sqrt{h}$
Receiver coordinates	Kinematic mode and estimated as random-walk with prior sigma of 100000 m and process noise 500 m for each station
Receiver clock	Estimate as white noise with prior sigma of 9000 m for each constellation
Ambiguity	Estimate as a constant and try to fixed for PPP-AR

determined. All possible subsets are traversed based on this number. The subsets are fixed using LAMBDA algorithm and selected with the maximum ratio value. In the second step, if the maximum value satisfies the ratio test, the PAR ends and the fixed solution is obtained. Otherwise, we increase the number of satellites to be deleted and repeat the first step. If the number of deleted ambiguities is greater than 5 or the remaining ambiguities are fewer than 5, the fixation process fails, and the float solution is output.

4. Kinematic PPP results

4.1. PPP float solution

The kinematic PPP is performed to investigate the contribution of ESAT1 on Multi-GNSS PPP solutions. For demonstration purpose, we selected one-hour data, 03:35:00–04:35:00, from DG07 station on DOY 1, 2023, as it shows the best enhancement performance. During the selected period, the ESAT1 can be continuously tracked for 6 min, among which the data with the elevation more than 10 degree last about 4 min. Fig. 4 illustrates the number of satellite tracks for each system throughout the specified time period. Afterwards, the float PPP results for all arcs of these stations are presented. In this study, once the horizontal and vertical positioning errors are less than 20 and 40 cm, respectively, and it lasts more than 150 epochs (about 5 min), the positioning is viewed as convergence for float PPP. The root mean square (RMS) of the converged positions is considered as the positioning accuracy. Table 3 lists the convergence time for the GNSS float PPP with or without ESAT1 at DG07 station during 03:35:00–04:35:00. The symbol "----" indicates that this solution did not converge. Subsequently, we conduct a detailed analysis of the contribution of ESAT1 satellite.

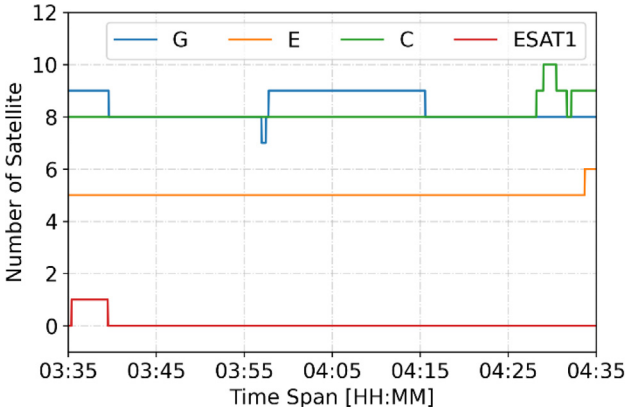

Fig. 4. Number of satellite tracked with elevation greater than 10° during 03:35:00–04:35:00, DOY 1, 2023.

For the single-constellation PPP, Fig. 5 illustrates the time series of the positioning errors as well as that of the ESAT1 enhanced solutions. The three subplots in each panel display the positioning errors in the east, north, and up direction. The left panel presents the results of

Table 3
The convergence time for the PPP determined with GNSS or its combination with ESAT1 at DG07 station during 03:35:00–04:35:00, DOY 1, 2023.

Constellation	GNSS [min]				GNSS + ESAT1 [min]			
	E	N	U	3D	E	N	U	3D
G	15.1	6.5	4.6	15.1	2.2	4.2	2.2	4.2
E	22.5	6.5	——	——	5.7	6.6	39.5	39.5
C	——	3.9	3.1	——	3.1	2.7	2.9	3.1
GE	13.3	4.8	3.9	13.3	2.2	4.6	3.8	4.6
GC	6.9	3.8	2.5	6.9	1.4	2.7	2.3	2.7
EC	11.6	6.2	2.6	11.6	2.5	5.1	2.1	5.1
GEC	6.9	4.8	2.2	6.9	1.5	3.9	3.1	3.9

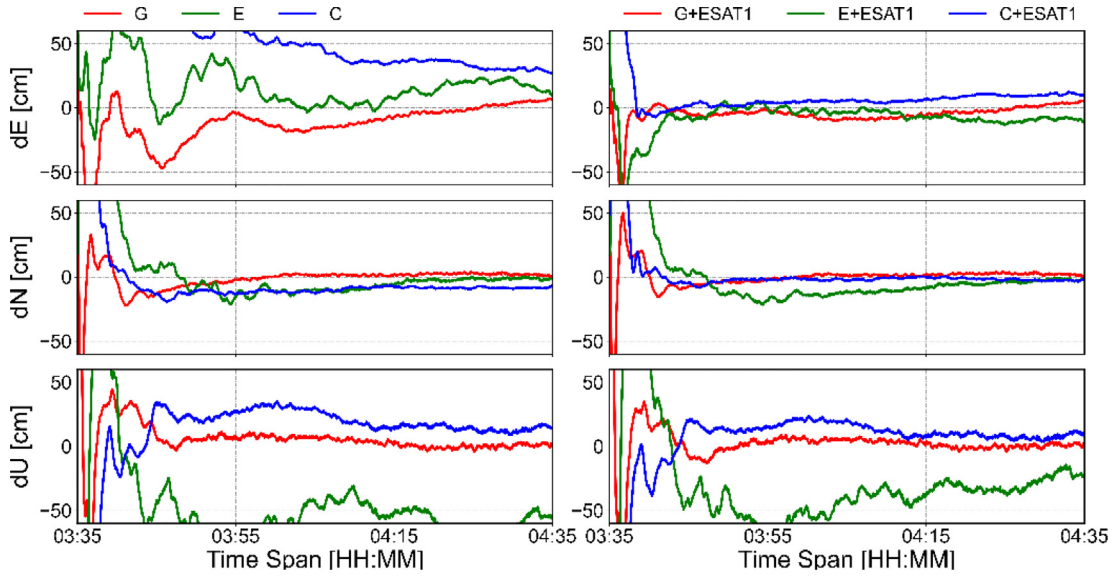

Fig. 5. The time series of the positioning errors in the east, north, and up direction for GPS, Galileo, and BDS only (left panel) as well as their LEO enhanced PPP solutions (right panel).

GPS- (red), Galileo- (green), and BDS-3 only (blue) PPP solutions, respectively. Their counterparts enhanced by ESAT1 are shown in the right panel with same colour. In general, the number of effective satellites for GPS, Galileo, and BDS-3 are 8.37, 5.02, and 8.13, respectively. The lowest number of Galileo satellite available is due to only 24 satellites deployed in orbit, compared to 32 GPS and 27 BDS-3 IGSO and MEO satellites. The average position dilution of precision (PDOP) values are 1.09, 1.51, and 1.13 for the three systems. By introduction of the ESAT1 satellite, the number of effective satellites as well as PDOP changes slightly, as the mission can only be tracked in relative short period. For the convergence time, the noticeable improvement can be observed in the east direction, whereas the effect is marginal in the north and up direction. It is well known that inclined LEO satellites significantly accelerate the geometrical configuration change of GNSS satellites in the eastward direction. Furthermore, the experiment involves just a single LEO experimental satellite, intensifying the enhancement performance in the eastward direction when compared to other directions. Therefore, our analysis focuses on the enhancement performance in the east direction.

With ESAT1 satellite, the convergence time of GPS, Galileo, and BDS PPP in the east direction is shortened from 15.0, 22.5, and more than 60 min to 2.2, 5.7, and 3.1 min, respectively. Moreover, the accuracy after convergence in the east direction is also improved from 9.9, 13.4, and 29.7 cm to 5.4, 7.2, and 6.7 cm. Among the three systems, the GPS achieves the fast convergence as well as best accuracy for both non– and LEO-enhanced PPP solutions in the east direction. The fewer number of effective satellites, only 5.02, prevents stable convergence of Galileo-only PPP. For BDS-3 only solution, noticeable improvement in the east direction can be observed once the ESAT1 is added.

We further investigate the PPP solutions with two constellations, i.e., GE, GC, and EC. Similarly, Fig. 6 presents the results with (left panel) and without (right panel) ESAT1 satellite. Compared to the single-constellation solution, the number of effective satellites has been increased, and the PDOP drops. The average number of effective satellites for these schemes are 13.39, 16.49, and 13.15, respectively. Among them, the GC scheme has the highest count, sequentially followed by GE and EC. The average PDOP values for these schemes are 0.87, 0.77, and 0.90,

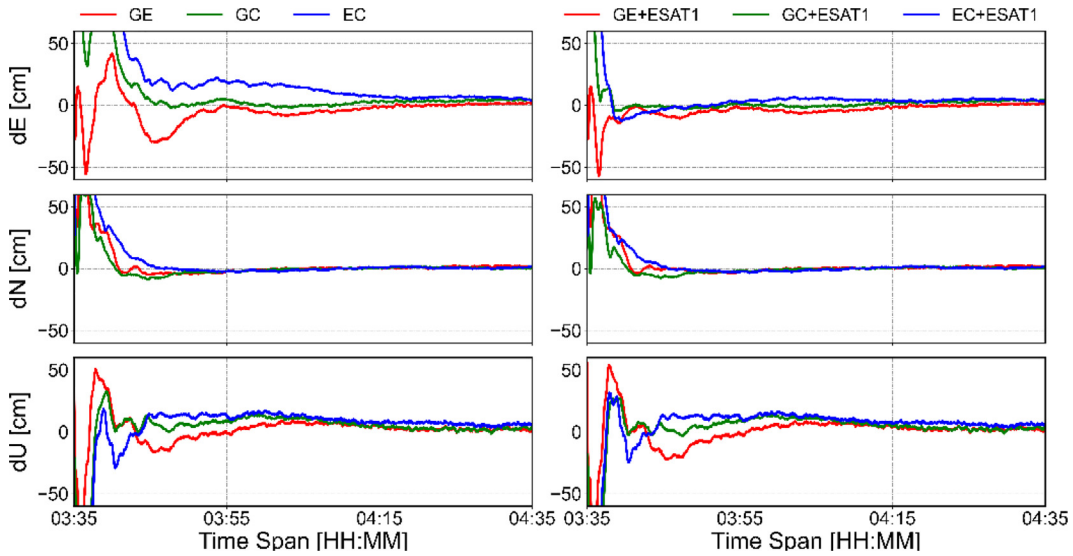

Fig. 6. The time series of the positioning errors in the east, north, and up direction for GPS + Galileo (GE), GPS + BDS (GC), and Galileo + BDS (EC) only as well as their LEO enhanced PPP solutions.

respectively. By adding the ESAT1 satellite, a significant improvement in the east direction can be observed. The similar phenomenon can be seen in the PPP with single constellation. The convergence time in the east direction is shortened from 13.3, 6.9, and 11.9 min to 2.2, 1.4, and 2.5 min, respectively. Moreover, the positioning accuracy in the east direction is also improved from 4.7, 4.4, and 12.4 cm to 3.5, 3.0, and 5.0 cm, respectively.

Fig. 7 illustrates the GPS, Galileo, and BDS combined solution. As all constellation are used, the average effective satellite number of 21.59 and a PDOP value of 0.68 are achieved. When ESAT1 satellite is used, the improvement of convergence and accuracy can also be observed, particularly in the east direction. Specifically, the convergence time in the east direction is reduced from 6.9 to 1.5 min, and the positioning accuracy is improved from 3.7 cm to 3.0 cm.

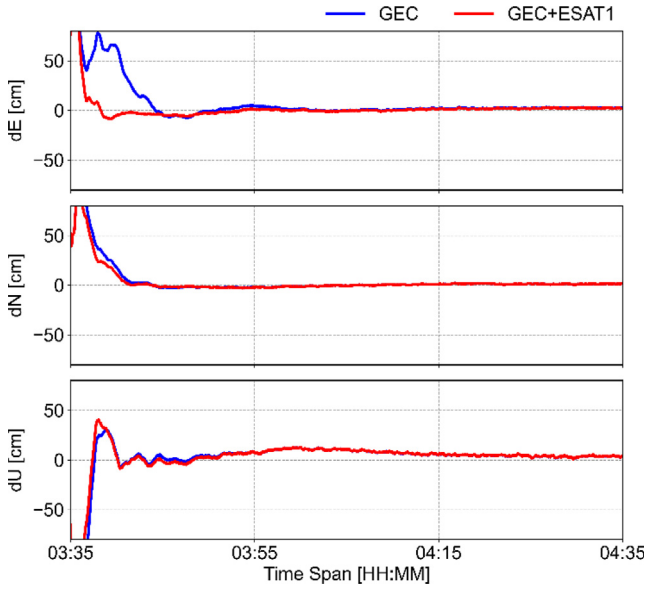

Fig. 7. The time series of the positioning errors in the east, north, and up directions for GPS + Galileo + BDS (GEC, blue) as well as their LEO enhanced PPP (red) solutions.

The statistical results on the convergence time for each PPP solutions of all ground tracking stations are illustrated in Fig. 8. Here only the effective LEO tracking arcs, a total of 23, are included for statistics. The effective arcs are defined as those with a tracking time of three minutes or more. Arcs without Mult-GNSS PPP convergence are also excluded from the statistical analysis. As shown in Fig. 8, the average convergence time for GPS, Galileo, and BDS-3 only PPP solutions is 21.2, 11.5, and 25.2 min, respectively. With ESAT1 satellite, the convergence times are reduced to 13.3, 9.1, and 13.2 min, equalling 37.3 %, 20.8 %, and 47.5 % improvement. Similarly, the average convergence time is reduced from 8.6, 12.4, and 8.7 min to 6.6, 9.0, and 6.1 min for GE, GC, and EC combined solutions, respectively. The percentage of improvement achieves 23.5 %, 27.3 %, and 29.5 %, respectively. In the case of all-system combined solution, the average convergence time is reduced from 7.3 to 6.0 min, and 17.4 % improvement can be observed. As aforementioned, the above analysis is based on the data with best performance. However, in average, the positive improvement can be observed from the statistic results.

Table 4 lists the accuracy after convergence for each scheme. The RMS in the east direction for GPS, Galileo, and BDS-3 only PPP solutions is 11.1, 11.4, and 14.5 cm, respectively. It can be reduced to 8.0, 8.8, and 10.1 cm further using the ESAT1 satellite with the improvement of 28 %, 23 % and 30 %. It should be noted that we set the convergence threshold of 20 cm and 40 cm for the horizontal and vertical direction. For the dual-system combined schemes, the eastward positioning accuracy is 6.6, 7.2, and 8.7 cm for GE, GC, and EC solutions, respectively.

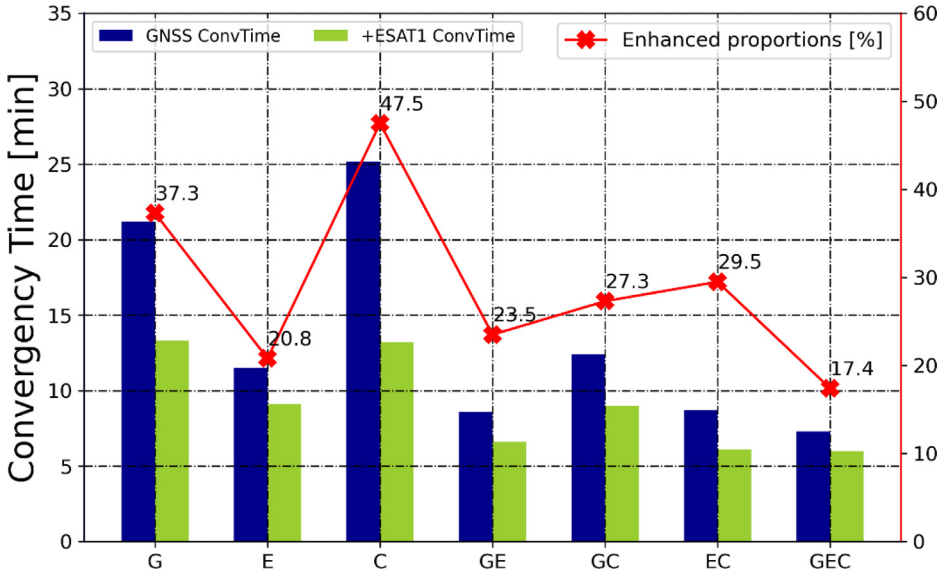

Fig. 8. Average convergence times of each PPP float solutions with (green) or without (navy blue) ESAT1 mission. The red dot line represents the percentage of reduction of the convergence time.

Table 4
The accuracy of float PPP solutions in kinematic mode with single-, dual-, and trip-constellation as well as CENTISPACE™ ESAT1 satellite. The percentage of improvements is also listed.

RMS	GNSS [cm]				GNSS + ESAT1 [cm]				Kinematic enhanced performance [%]			
	E	N	U	3D	E	N	U	3D	E	N	U	3D
G	11.1	8.0	14.3	19.8	8.0	6.5	13.0	16.6	28	19	9	16
E	11.4	7.0	15.9	20.8	8.8	5.6	13.0	16.7	23	20	18	20
C	14.5	5.2	16.6	22.6	10.1	4.5	12.6	16.8	30	13	24	26
GE	6.6	4.2	9.9	12.6	6.2	4.2	8.7	11.5	6	0	12	9
GC	7.2	4.4	9.8	12.9	6.9	4.0	9.8	12.6	4	9	0	2
EC	8.7	4.6	10.1	14.1	7.1	4.2	9.5	12.6	18	9	6	11
GEC	6.6	3.7	10.5	12.9	5.9	3.6	10.2	12.3	11	3	3	5

With the aid of ESAT1 satellite, the positioning accuracies are improved 6 %, 4 %, and 18 % further to 6.2, 6.9, and 7.1 cm. In the case of all-system combined scheme, the eastward accuracy is improved from 6.6 to 5.9 cm, about 11 %. Compared to the east direction, accuracy improvements in the north and up direction is weak, which is consisted with the above analysis. In terms of 3D accuracy, the single-system solutions show 16 %, 20 %, and 26 % improvement, respectively. As for the combined schemes, the 3D accuracy is also improved with the augmentation of ESAT1. In general, the single-system solution is significantly better than the combined solution in terms of enhancement performance.

4.2. PPP-AR solution

Ambiguity resolution is essential to improve positioning accuracy of PPP and accelerate the convergence. The quality of float ambiguity solution helps ambiguity resolution. As demonstrated in the previous section, the inclusion of ESAT1 satellite has significantly enhanced the performance of the floating solution in both accuracy as well as convergence. This section aims to explore the impact of ESAT1 on Multi-GNSS PPP-AR. As station 6229 has poor tracking capability of GNSS, we exclude it and the arcs of stations 6101, 6102, 6103, DG04, DG06, and DG07, in the total of 20 solutions, were processed with the same schemes as that for PPP in the previous section.

Based on 135 IGS reference stations distributed globally, the multi-GNSS Observable-specific Signal Bias (OSB) products are solved based on the WUM products and used for PPP-AR. The influence of ESAT1 on ambiguity fixed solution is analyzed based on the matrices of success fix rate and TTFF. Here, the successful fixed solution is defined as the periods of TTFF less than 1 h, and the success fix rate is defined as the ratio of the number with success fixed solutions to the total number of solutions (Hong et al., 2023). The TTFF is defined as the time difference between the beginning epoch and the epoch when a fixed solution of less than 10 cm in the horizontal and vertical components is achieved and it lasts for 20 consecutive epochs at least. The criterion of TTFF differs from that of convergence of float PPP above.

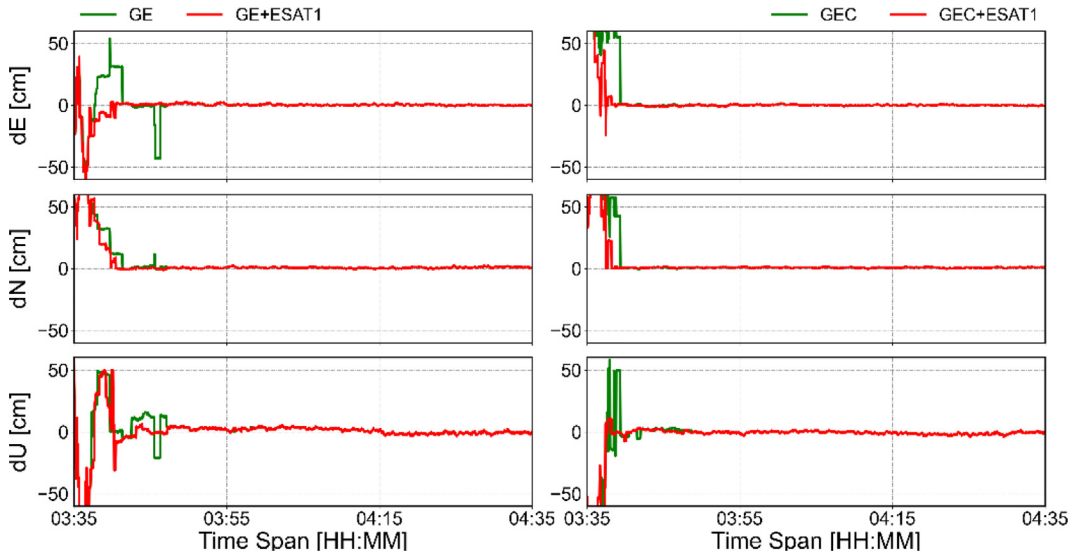

Fig. 9. The time series of the positioning errors in the east, north, and up directions for GE/GEC (green) as well as their LEO enhanced (red) PPP-AR solutions at DG07 station during 03:35:00–04:35:00, DOY 1, 2023.

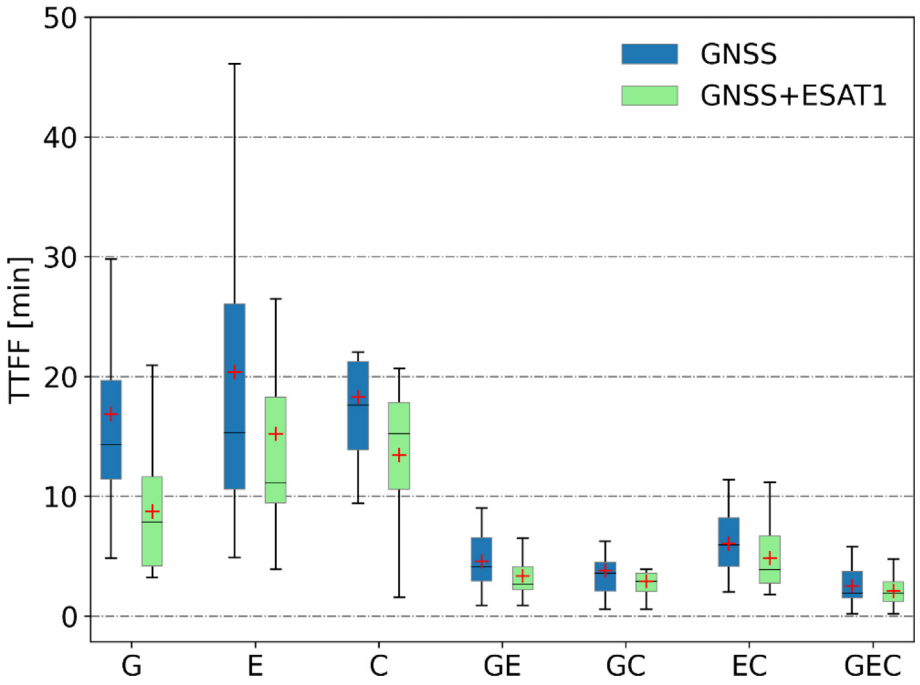

Fig. 10. TTFF distribution of PPP-AR for each scheme. The box is divided into three parts: the upper boundary (Q3 quantile), the middle groove (median) and the lower boundary (Q1 quantile). The length of the entire box is inter-quartile range (IQR). The lower and upper short lines of the box extension represent the minimum and maximum, respectively. The red marker '+' indicates the mean TTFF.

Fig. 9 illustrates the positioning errors for GE and GEC PPP-AR, as well as the positioning errors for the ESAT1 enhanced solutions at DG07 station during 03:35:00–04:35:00. The TTFF for the GE and GEC PPP-AR schemes are 12.13 and 4.40 min, respectively. It is evident that the BDS system plays a crucial role in achieving fast GNSS convergence. With the assistance of ESAT1, the convergence time is reduced to 5.53 and 3.23 min.

Due to the limitation of satellite number and distribution of single constellation, the convergence of the float solution is relatively longer, resulting in the longer time for successful ambiguity resolution. As shown in Fig. 10, the TTFF of single-system is much slower than that of combined solutions due to its poorer geometric configuration. With the increase of GNSS constellations, the TTFF is further reduced. Furthermore, Table 5 lists the success fix

Table 5
The success fix rate and mean TTFF for each solution with or without ESAT1. The improved percentage are also given.

Solutions	Success fix rate [%]		Mean TTFF [min]		Improved percentage [%]
	GNSS	GNSS + ESAT1	GNSS	GNSS + ESAT1	
G	100	100	16.8	8.7	48.2
E	90	95	20.4	15.2	25.3
C	65	70	18.3	13.4	26.6
GE	100	100	4.6	3.3	27.1
GC	100	100	3.8	2.9	24.2
EC	100	100	6.0	4.9	19.6
GEC	100	100	2.5	2.1	17.8

rate, mean TTFF, and the percentage of improved solutions. It is important to note that the BDS only solution has a fixed success rate of 65 % due to too many cycle-slip in the tracking process at stations 6101 and 6102. These results in frequent reconvergence, degenerating the performance. In addition, the mean TTFF for GPS-, Galileo- and BDS-only is 16.8, 20.4 and 18.3 min, respectively, and can be further shortened to 8.7, 15.2, and 13.4 min with the aid of ESAT1. Specifically, the mean TTFF is shortened by 48.2 %, 25.3 %, and 26.6 % for each single system. Similarly, for the combined GE, GC, and EC schemes, the average TTFF experiences a reduction from 4.6, 3.8, and 6.0 min to 3.3, 2.9, and 4.9 min, respectively. Around 27.1 %, 24.2 %, and 19.6 % improvement has been achieved, respectively. In the GEC combination solution, a significant reduction in average TTFF is observed from 2.5 to 2.1 min (17.8 % improvement). Overall, the contribution of the ESAT1 satellite to GNSS PPP-AR is noticeable.

5. Conclusion

With the fast motion of LEO satellites and the rapid change of geometric configuration, LEO is one of the important means to accelerate PPP convergence. This study presents a unified PPP model with Multi-GNSS and LEO constellation in an undifferenced and ionosphere-free combination. The real tracking data from ground stations for CENTISPACE^{TM} ESAT1 LEO satellite is used to investigate and assess the possibility and contribution of LEO satellites on the convergence and accuracy of PPP with Multi-GNSS observation. Basic information of the CENTISPACE^{TM} LEO constellation, ground tracking data and processing strategy are presented. It should be noted that the constellation is capable of transmitting GNSS-compatible navigation signals. Further, the performance of Multi-GNSS PPP and PPP-AR augmented with the ESAT1 satellite is studied and analyzed, with focus on convergence time and accuracy.

To demonstrate the contribution of the ESAT1 satellite to kinematic PPP, we carefully select a one-hour dataset. The results reveal that the ESAT1 satellite make the most significant contribution to eastward convergence. The results from effective arcs of all stations also confirm the finds. Specifically, using the ESAT1 satellite, the convergence time of PPP float solutions of G/E/C/GE/GC/EC/GEC can be reduced by 37.3 %, 20.8 %, 47.5 %, 23.5 %, 27.3 %, 29.5 %, and 17.4 %, respectively. Furthermore, the positioning accuracy shows significant improvement. The contribution to PPP-AR is also investigated. With the OSB solved with 135 global stations, the influence of the ESAT1 satellite on GNSS PPP-AR is assessed. By combining the observations from the ESAT1 satellite and Multi-GNSS, the average TTFF of G/E/C/GE/GC/EC/GEC solutions is reduced about 48.2 %, 25.3 %, 26.6 %, 27.1 %, 24.2 %, 19.6 %, and 17.8 %, respectively. The promising results in both float PPP and PPP-AR can be obtained in our experiment, although only one LEO satellite is used to enhance the Multi-GNSS PPP, which demonstrates the positive contribution of LEO on positioning. It can be expected to obtain better performance when the LEO constellation is completely constructed in the future.

Declaration of competing interest

The authors declare that they have no known competing financial interests or personal relationships that could have appeared to influence the work reported in this paper.

Acknowledgements

We are grateful to the Editor in Chief Pascal Willis and three anonymous reviewers for their helpful suggestions and valuable comments. This study is financially supported by the National Natural Science Foundation of China (42304032, 41974035), Yong Elite Scientists Sponsorship Program by China Association of Science and Technology (2018QNRC001), the Fundamental Research Funds for the Central Universities (2042021kf0065), and China Postdoctoral Science Foundation, (2020M682483). The authors would like to acknowledge the Beijing Future Navigation Tech Co., Ltd., for providing the LEO augmentation data, and the ESAT1 augmentation data is under restrictions of Beijing Future Navigation Tech Co., Ltd., and can be available from the corresponding author upon reasonable request and with permission of Beijing Future Navigation Tech Co., Ltd.

References

Blewitt, G., 1990. An automatic editing algorithm for GPS data. Geophys. Res. Lett. 17, 199–202. https://doi.org/10.1029/GL017i003p00199.

Chobotov, V.A. (Ed.), 2002. Orbital mechanics, 3rd ed. ed, AIAA education series. American Institute of Aeronautics and Astronautics, Reston, Va.

CNAGA, 2017. CASIC Plans to Launch 156 Small Satellites for the Hongyun Program - news | China National Administration of GNSS and Applications CNAGA chinabeidou.gov.cn [WWW Document]. URL http://en.beidouchina.org.cn/c/393.html (accessed 4.7.23).

Selding, P.B. de, 2016. Boeing proposes big satellite constellations in V- and C-bands. SpaceNews. URL https://spacenews.com/boeing-proposes-big-satellite-constellations-in-v-and-c-bands/ (accessed 4.7.23).

Dong, D., Bock, Y., 1989. Global Positioning System Network analysis with phase ambiguity resolution applied to crustal deformation studies in California. J. Geophys. Res. Solid Earth 94, 3949–3966. https://doi.org/10.1029/JB094iB04p03949.

Enge, P., Ferrell, B., Bennett, J., Whelan, D., Gutt, G., Lawrence, D., 2012. Orbital Diversity for Satellite Navigation. In: Presented at the Proceedings of the 25th International Technical Meeting of the Satellite Division of The Institute of Navigation (ION GNSS 2012), pp. 3834–3846.

Fossa, C.E., Raines, R.A., Gunsch, G.H., Temple, M.A., 1998. An overview of the IRIDIUM (R) low Earth orbit (LEO) satellite system. In: Proceedings of the IEEE 1998 National Aerospace and Electronics Conference. NAECON 1998. Celebrating 50 Years (Cat. No.98CH36185). Presented at the Proceedings of the IEEE 1998 National Aerospace and Electronics Conference. NAECON 1998. Celebrating 50 Years (Cat. No.98CH36185), pp. 152–159. https://doi.org/10.1109/NAECON.1998.710110.

Ge, H., Li, B., Ge, M., Zang, N., Nie, L., Shen, Y., Schuh, H., 2018. Initial assessment of precise point positioning with LEO enhanced global navigation satellite systems (LeGNSS). Remote Sens. 10, 984. https://doi.org/10.3390/rs10070984.

Ge, H., Li, B., Jia, S., Nie, L., Wu, T., Yang, Z., Shang, J., Zheng, Y., Ge, M., 2022. LEO enhanced Global Navigation Satellite System (LeGNSS): progress, opportunities, and challenges. Geo-Spat. Inf. Sci. 25, 1–13. https://doi.org/10.1080/10095020.2021.1978277.

Guo, J., Wang, C., Chen, G., Xu, X., Zhao, Q., 2023. BDS-3 precise orbit and clock solution at Wuhan University: status and improvement. J. Geod. 97, 15. https://doi.org/10.1007/s00190-023-01705-5.

Harebottle, 2018. Comtech, Kepler to Drive Rapidly Deployable LEO Comms [WWW Document]. URL https://www.satellitetoday.com/telecom/2018/06/06/comtech-kepler-to-drive-rapidly-deployable-leo-comms/ (accessed 4.7.23).

Hill, 2020. Maxar Stock Surges on Strong 2Q, Executives Update Legion, Telesat LEO Outlook [WWW Document]. URL https://www.satellitetoday.com/business/2020/08/06/maxar-stock-surges-on-strong-2q-executives-update-legion-telesat-leo-outlook/ (accessed 4.7.23).

Hong, J., Tu, R., Zhang, P., Zhang, R., Han, J., Fan, L., Wang, S., Lu, X., 2023. GNSS rapid precise point positioning enhanced by low Earth orbit satellites. Satell. Navig. 4, 11. https://doi.org/10.1186/s43020-023-00100-x.

Jewett, 2020. FCC Grants OneWeb Market Access for 2,000-Satellite Constellation [WWW Document]. URL https://www.satellitetoday.com/broadband/2020/08/26/fcc-grants-oneweb-market-access-for-2000-satellite-constellation/ (accessed 4.7.23).

Jones, 2018. Chinese rocket maker OneSpace secures $44m in funding; Expace prepares for commercial launch [WWW Document]. URL https://spacenews.com/chinese-rocket-maker-onespace-secures-44m-in-funding-expace-prepare-for-commercial-launch/ (accessed 4.7.23).

Ke, M., Lv, J., Chang, J., Dai, W., Tong, K., Zhu, M., 2015. Integrating GPS and LEO to accelerate convergence time of precise point positioning. In: 2015 International Conference on Wireless Communications & Signal Processing (WCSP). Presented at the 2015 International Conference on Wireless Communications & Signal Processing (WCSP), pp. 1–5. https://doi.org/10.1109/WCSP.2015.7341230.

Li, X., Ma, F., Li, X., Lv, H., Bian, L., Jiang, Z., Zhang, X., 2019b. LEO constellation-augmented multi-GNSS for rapid PPP convergence. J. Geod. 93, 749–764. https://doi.org/10.1007/s00190-018-1195-2.

Li, B., Shen, Y., Feng, Y., Gao, W., Yang, L., 2014. GNSS ambiguity resolution with controllable failure rate for long baseline network RTK. J. Geod. 88, 99–112. https://doi.org/10.1007/s00190-013-0670-z.

Li, B., Ge, H., Ge, M., Nie, L., Shen, Y., Schuh, H., 2019a. LEO enhanced Global Navigation Satellite System (LeGNSS) for real-time precise positioning services. Adv. Space Res. 63, 73–93. https://doi.org/10.1016/j.asr.2018.08.017.

Li, M., Xu, T., Guan, M., Gao, F., Jiang, N., 2022a. LEO-constellation-augmented multi-GNSS real-time PPP for rapid re-convergence in harsh environments. GPS Solut. 26, 29. https://doi.org/10.1007/s10291-021-01217-9.

Li, Z., Xu, G., Guo, J., Zhao, Q., 2022b. A sequential ambiguity selection strategy for partial ambiguity resolution during RTK positioning in urban areas. GPS Solut. 26, 92. https://doi.org/10.1007/s10291-022-01279-3.

Magan, 2015. Samsung Exec Envisions LEO Constellation for Satellite Internet Connectivity [WWW Document]. URL https://www.satellitetoday.com/telecom/2015/08/18/samsung-exec-envisions-leo-constellation-for-satellite-internet-connectivity/ (accessed 4.7.23).

McDowell, J.C., 2020. The low earth orbit satellite population and impacts of the SpaceX starlink constellation. Astrophys. J. 892, L36. https://doi.org/10.3847/2041-8213/ab8016.

Meng, Y., L. Bian, Y. Wang, T. Yan, W. Lei, M. He, and X. Li., 2018. Global Navigation Augmentation System Based on Hongyan Satellite Constellation [WWW Document]. URL https://www.cnki.com.cn/Article/CJFDTotal-GJTK201810005.htm (accessed 4.7.23).

Nyirady A, 2019a. Astrome Launches ICO, Gearing up for LEO Constellation [WWW Document]. URL https://www.satellitetoday.com/innovation/2019/08/15/astrome-launches-ico-gearing-up-for-leo-constellation/ (accessed 4.7.23).

Nyirady A, 2019b. Astrocast Signs Launch Agreement With D-Orbit [WWW Document]. URL https://www.satellitetoday.com/launch/2019/10/30/astrocast-signs-launch-agreement-with-d-orbit/ (accessed 4.7.23).

Parkins, A., 2011. Increasing GNSS RTK availability with a new single-epoch batch partial ambiguity resolution algorithm. GPS Solut. 15, 391–402. https://doi.org/10.1007/s10291-010-0198-0.

Reid, T.G., Neish, A.M., Walter, T.F., Enge, P.K., 2016. Leveraging Commercial Broadband LEO Constellations for Navigating. Presented at the Proceedings of the 29th International Technical Meeting of the Satellite Division of The Institute of Navigation (ION GNSS+ 2016), pp. 2300–2314. https://doi.org/10.33012/2016.14729.

Reid, T.G.R., Walter, T., Enge, P.K., Sakai, T., 2016b. Orbital representations for the next generation of satellite-based augmentation systems. GPS Solut. 20, 737–750. https://doi.org/10.1007/s10291-015-0485-x.

Saastamoinen, J., 1972. Contributions to the theory of atmospheric refraction. Bull. Géod. 105, 279–298. https://doi.org/10.1007/BF02521844.

Teunissen, P.J.G., 1995. The least-squares ambiguity decorrelation adjustment: a method for fast GPS integer ambiguity estimation. J. Geod. 70, 65–82. https://doi.org/10.1007/BF00863419.

Wang, L., Chen, R., Xu, B., Zhang, X., Li, T., Wu, C., 2019. The Challenges of LEO Based Navigation Augmentation System – Lessons Learned from Luojia-1A Satellite. In: Sun, J., Yang, C., Yang, Y. (Eds.), China Satellite Navigation Conference (CSNC) 2019 Proceedings, Lecture Notes in Electrical Engineering. Springer Singapore, Singapore, pp. 298–310. https://doi.org/10.1007/978-981-13-7759-4_27.

Zhao, Q., Pan, S., Gao, C., Gao, W., Xia, Y., 2020. BDS/GPS/LEO triple-frequency uncombined precise point positioning and its performance in harsh environments. Measurement 151, 107216. https://doi.org/10.1016/j.measurement.2019.107216.

Zheng, Y., Ge, H., Li, B., 2023. The convergence mechanism of Low Earth Orbit enhanced GNSS (LeGNSS) Precise Point Positioning (PPP). Geo-Spat. Inf. Sci. 1–16. https://doi.org/10.1080/10095020.2023.2270712.